The estimate of sensitivity for large infrared telescopes based on measured sky brightness and atmospheric extinction

Zhi-Jun Zhao (赵志军)[1,4], Hai-Jing Zhou (周海静)[1], Yu-Chen Zhang (张雨辰)[2], Yun Ling (凌云)[3] and Fang-Yu Xu (许方宇)[2]*

[1] School of Physics, Henan Normal University, Xinxiang 453007, China; *xu_fangyu@ynao.ac.cn; zhaozhijun@htu.edu.cn*
[2] Yunnan Observatories, Chinese Academy of Sciences, Kunming 650216, China
[3] Kunming Institute of Physics, Kunming 650216, China
[4] Henan Key Laboratory of Infrared Materials & Spectrum Measures and Applications, Xinxiang 453007, China

Abstract In order to evaluate the ground-based infrared telescope sensitivity affected by the noise from the atmosphere, instruments and detectors, we construct a sensitivity model that can calculate limiting magnitudes and signal-to-noise ratio (S/N). The model is tested with tentative measurements of M'-band sky brightness and atmospheric extinction obtained at the Ali and Daocheng sites. We find that the noise caused by an excellent scientific detector and instruments at $-135°C$ can be ignored compared to the M'-band sky background noise. Thus, when $S/N = 3$ and total exposure time is 1 second for 10 m telescopes, the magnitude limited by the atmosphere is 13.01^m at Ali and 12.96^m at Daocheng. Even under less-than-ideal circumstances, i.e., the readout noise of a deep cryogenic detector is less than $200\ e^-$ and the instruments are cooled to below $-87.2°C$, the above magnitudes decrease by 0.056^m at most. Therefore, according to observational requirements with a large telescope in a given infrared band, astronomers can use this sensitivity model as a tool for guiding site surveys, detector selection and instrumental thermal-control.

Key words: methods: miscellaneous — atmospheric effects — telescopes — site testing — instrumentation: detectors — instrumentation: miscellaneous

1 INTRODUCTION

Infrared observations have unique advantages in astronomical research such as observing cool celestial objects and extra-solar planets. Many 8–10 m ground-based telescopes (Keck, Gemini, Subaru, etc) are equipped with infrared instruments. Currently, a 12 m optical infrared telescope and an 8 m solar telescope scheduled to be built in China will be equipped with infrared instruments (Cui et al. 2018; Deng et al. 2016; Liu et al. 2012). On the ground, the sensitivity of large telescopes is affected by sky background, atmospheric extinction, detector noise, and instrumental noise.

The sky background and atmospheric extinction set a fundamental sensitivity limit of infrared observations, so they are key indicators in site surveys of large infrared telescopes. From the 1970s to 1990s, the 1 μm ∼ 30 μm infrared sky brightness was widely

measured abroad (Westphal 1974; Ashley et al. 1996; Smith & Harper 1998; Phillips et al. 1999). In China, site surveys have been carried out for many years on the dry and cold western plateau, and three excellent sites (Ali site in Tibet, Daocheng site in Sichuan, and Muztagh Ata in Xinjiang) have been listed as the candidates for large optical/infrared telescopes (Yao 2005; Wu et al. 2016; Song et al. 2020a,b; Feng et al. 2020). By continuously measuring air-temperature and water vapor content (Qian et al. 2015; Wang et al. 2013; Liu et al. 2018), astronomers find that the three sites may be suitable for infrared observations. Nevertheless, direct evidence that reflects the quality of sites used for infrared observations is scarce. The near-infrared (J, H and K band) sky brightness at the Ali site has been measured with an InGaAs detector since 2017 (Dong et al. 2018; Tang et al. 2018; Wang et al. 2018). The M'-band sky brightness and atmospheric transmittance were tentatively measured at the Daocheng site in March 2017 and Ali site

---

⋆ Corresponding author

in October 2017 (Zhao 2017; Wang et al. 2020). In the thermal infrared such as M′-band, even if the best sites for large telescopes have been indicated by measuring sky brightness and atmospheric extinction, it is also essential to strictly control the instrumental thermal-emission and detector noise in order to approach the fundamental sensitivity limit of infrared observations at the excellent sites. Hence, we need to study the various noise sources causing observational errors and determine the condition that the noise of the detectors and instruments can fulfill the required sensitivity of observations.

In this paper, we analyze the impact of various noise sources on the ground-based infrared telescope sensitivity, and then try to provide reasonable suggestions for detector selection and instrumental thermal-control. In Section 2, we construct a sensitivity model that can be used to calculate the signal-to-noise ratio (S/N) and limiting magnitudes. In order to quantitatively describe the impact of noise caused by detectors and instruments on the S/N, we define a physical quantity called the quality factor (Q_{snr}) of the signal-to-noise ratio. In Section 3, we provide tentative measurements of M′-band sky brightness and atmospheric extinction obtained at the Ali and Daocheng sites. In Section 4 by using the above measurements, we calculate the M′-band limiting magnitudes of 10 m telescopes and discuss the noise distribution and instrumental thermal-control. In Section 5, final conclusions are summarized.

2 THE SENSITIVITY MODEL BASED ON SKY BRIGHTNESS AND ATMOSPHERIC EXTINCTION

2.1 The Signal-to-Noise Ratio (S/N) and the Exo-Atmospheric Magnitude

In astronomical observations, noise is usually caused by fluctuations of electron numbers produced by a signal and background. The signal may be from a star, and the background generally consists of sky background, instrumental background, dark current, and readout noise. In order to find an accurate signal the background needs to be subtracted. However, in the thermal infrared the background is hard to accurately subtract because it usually fluctuates rapidly. Thus, the variance of the background noise may be added twice into the total noise variance (Léna et al. 2012). Hence, the standard deviation of a fluctuating signal and background, which typically obeys a Poisson distribution, can be expressed as Equation (1):

$$\sigma = \sqrt{Sig \cdot t + 2[B_{sky} \cdot t + B_{ins} \cdot t + n_{pixel} \cdot (Dark \cdot t + Ron^2)]}, \tag{1}$$

where Sig is the signal electrons per second, B_{sky} is the electrons per second from the sky background, B_{ins} is the electrons per second from the total instrumental background containing the emission from a telescope and relay optics, t is the elementary exposure time in seconds for the detector, $Dark$ is the dark electrons per second at a unit pixel, Ron is the RMS readout noise per pixel, and n_{pixel} is the number of pixels covered by a star image.

The S/N is shown in Equation (2):

$$\begin{aligned}
\frac{S}{N} &= \frac{n_f \cdot Sig \cdot t}{\sqrt{n_f} \cdot \sigma} \\
&= \sqrt{Sig \cdot n_f \cdot t} \\
&\quad \sqrt{\frac{Sig \cdot t}{Sig \cdot t + 2[B_{sky} \cdot t + B_{ins} \cdot t + n_{pixel} \cdot (Dark \cdot t + Ron^2)]}} \\
&= \sqrt{n_f \cdot t}\sqrt{\frac{B_{sky}}{\beta}}\sqrt{\frac{1}{1 + 2(\beta + \beta \cdot \alpha_1 + \beta \cdot \alpha_2)}},
\end{aligned} \tag{2}$$

where $\beta = B_{sky}/Sig$, $\alpha_1 = B_{ins}/B_{sky}$, $\alpha_2 = n_{pixel} \cdot (Dark \cdot t + Ron^2)/(B_{sky} \cdot t)$, n_f is the number of superposed frames in multi-frame techniques, and $n_f \cdot t$ can be viewed as the total exposure time.

In Equation (2), the Sig, B_{sky} and B_{ins} in a given wave-band can be calculated by

$$Sig = \tau_{atm}\tau_{ins}\eta F_{sig}\pi(\frac{D}{2})^2\frac{\lambda}{hc}, \tag{3}$$

$$B_{sky} = \tau_{ins}\eta L_{sky}\pi(\frac{D}{2})^2\Omega_{star}\frac{\lambda}{hc}, \tag{4}$$

$$B_{ins} = \eta L_{ins}\pi(\frac{D}{2})^2\Omega_{star}\frac{\lambda}{hc}. \tag{5}$$

In Equations (3), (4) and (5), τ_{atm} is the atmospheric transmittance, τ_{ins} is the total instrumental transmittance, η is the quantum efficiency of a detector, F_{sig} is the flux of a star, L_{sky} is the sky brightness, L_{ins} is the radiance of instruments, Ω_{star} is the solid angle subtended by the image of a star, D is the telescope diameter, h is the Plank constant, c is the velocity of light, and λ is wavelength.

In Equations (4) and (5), the L_{sky} and the L_{ins} can be obtained by measurement or simulation. Based on the black-body radiation theory, for any object another form of radiance can also be expressed by

$$L_{obj} = \epsilon_{obj} \cdot L_{obj}^b = \epsilon_{obj}^* \cdot L_{amb}^b, \tag{6}$$

where ϵ_{obj} is the real emissivity, ϵ_{obj}^* is the effective emissivity, L_{obj} is the radiance of an object, L_{obj}^b is the black-body radiance at the object's temperature, and L_{amb}^b is black-body radiance at the ambient temperature. By using the effective emissivity a more convenient form of α_1 can be rewritten by

$$\alpha_1 = \frac{B_{ins}}{B_{sky}} = \frac{\epsilon_{ins}^* \cdot L_{amb}^b}{\tau_{ins} \cdot \epsilon_{sky}^* \cdot L_{amb}^b} = \frac{\epsilon_{ins}^*}{\tau_{ins} \cdot \epsilon_{sky}^*}, \tag{7}$$

where $\epsilon_{\mathrm{sky}}^*$ is the effective emissivity of sky, and $\epsilon_{\mathrm{ins}}^*$ is the effective emissivity of the instruments.

From Equations (3) and (4), F_{sig} can be expressed by

$$F_{\mathrm{sig}} = \frac{L_{\mathrm{sky}} \cdot \Omega_{\mathrm{star}}}{\beta \cdot \tau_{\mathrm{atm}}}. \tag{8}$$

Then the exo-atmospheric magnitude of the stellar flux is obtained by

$$\begin{aligned} m_{\mathrm{sig}} &= -2.5\log_{10}(\frac{F_{\mathrm{sig}}}{F_0 \times \Delta\lambda}) \\ &= -2.5\log_{10}(\frac{L_{\mathrm{sky}} \cdot \Omega_{\mathrm{star}}}{\beta \cdot \tau_{\mathrm{atm}}} \cdot \frac{1}{F_0 \times \Delta\lambda}), \end{aligned} \tag{9}$$

where F_0 is the spectral flux of zero magnitude in a given wave-band, and $\Delta\lambda$ is the bandwidth of filter.

Obviously, if the sky brightness and the atmospheric extinction at astronomical sites are given, the relationship between S/N or m_{sig} and β can be easily obtained by Equation (2) or (9). Thus, for any S/N, m_{sig} can be calculated.

2.2 The Quality Factor of the Signal-to-Noise Ratio

In the infrared observations on the ground, the detector noise and the instrument noise make the S/N always lower than its theoretical limit (TL) determined by sky background and stellar intensity. In order to quantitatively describe the impact of noise caused by detectors and instruments on the S/N, it is necessary to introduce a physical quantity which can express the decrease of S/N. From the foregoing discussion we find that when $(\alpha_1 + \alpha_2) \to 0$, S/N reaches its TL. Thus, we obtain Equation (10):

$$\frac{S}{N}\Big|_{\mathrm{TL}} = \lim_{(\alpha_1+\alpha_2)\to 0} \frac{S}{N} = \sqrt{n_f \cdot t}\sqrt{\frac{B_{\mathrm{sky}}}{\beta}}\sqrt{\frac{1}{1+2\beta}}. \tag{10}$$

According to Equations (2) and (10) a physical quantity Q_{snr} called the quality factor of S/N can be defined as follows using Equation (11):

$$Q_{\mathrm{snr}} = \frac{\frac{S}{N}}{\frac{S}{N}|_{\mathrm{TL}}} = \frac{\sqrt{1+2\beta}}{\sqrt{1+2\beta+2\beta(\alpha_1+\alpha_2)}}. \tag{11}$$

Obviously, $0 < Q_{\mathrm{snr}} < 1$. The larger Q_{snr} is, the better is the sensitivity of the telescope. For the given β and Q_{snr} in Equation (11), $\alpha_1 + \alpha_2$ can be calculated with Equation (12):

$$\alpha_1 + \alpha_2 = (\frac{1}{Q_{\mathrm{snr}}^2} - 1)(1 + \frac{1}{2\beta}). \tag{12}$$

From Equations (10), (11) and (12), one can obtain the following facts for a given sky background:

(1) For $2\beta \ll 1$, $S/N|_{\mathrm{TL}} \approx \sqrt{n_f \cdot t \cdot B_{\mathrm{sky}}/\beta} \propto \beta^{-1/2}$. The intensity of the stellar flux is far greater than the sky background, and the sensitivity is limited by the signal shot noise.

(2) For $2\beta \gg 1$, which is called the background-limited domain, $\alpha_1 + \alpha_2 \approx (Q_{\mathrm{snr}}^{-2} - 1)$ and $S/N|_{\mathrm{TL}} \approx \sqrt{n_f \cdot t \cdot B_{\mathrm{sky}}/2}/\beta \propto \beta^{-1}$. We take the partial derivative of $S/N|_{\mathrm{TL}}$ with respect to β, and then obtain $\partial(S/N|_{\mathrm{TL}})/(S/N|_{\mathrm{TL}}) = \partial\beta/\beta$. Likewise, taking the partial derivative of the m_{sig} in Equation (9) with respect to β, we can obtain $\partial(m_{\mathrm{sig}}) = 2.5 \times \log_{10}(e) \times \partial\beta/\beta$. Thus, in this domain, the slight reduction relative to the magnitude limited by sky background can be approximately obtained by

$$\Delta m_{\mathrm{sig}} \approx 2.5\times\log_{10}(e)\times\frac{\Delta(\frac{S}{N}|_{\mathrm{TL}})}{\frac{S}{N}|_{\mathrm{TL}}} = 1.086\times(1-Q_{\mathrm{snr}}). \tag{13}$$

Based on the desired Δm_{sig}, Equation (13) can be used to roughly estimate Q_{snr}. However, this only applies to the circumstances where S/N approaches TL. By combining Equations (12) and (13), we can use Q_{snr} to obtain reasonable requirements for detector noise and instrument noise. Thus, according to the Q_{snr}, the background-limited condition of astronomical sites (BLCAS) can be defined mathematically as

$$\begin{cases} 2\beta \gg 1 \\ Q_{\mathrm{snr}} \to 1 \end{cases}. \tag{14}$$

As illustrated in Equation (13), if we can accept that the maximum magnitude reduction with respect to the magnitude limited by sky background is about 0.05^{m}, the minimum of Q_{snr} should be about 0.95. Hence, in the background limited domain, the upper limit of $\alpha_1 + \alpha_2$ is 0.11, which determines the maximum noise allowed from instruments and detectors.

3 THE MEASUREMENTS OF M′-BAND SKY BRIGHTNESS AND ATMOSPHERIC EXTINCTION

Between 2015 and 2017 an atmospheric mid-infrared radiation meter (AMIRM) was developed by Yunnan Observatories and Kunming Institute of Physics. With the AMIRM, we measured the M′-band sky brightness and atmospheric extinction at the 4750 m Daocheng site ($29.107°$ north, $100.109°$ east) in late March 2017, and at the 5100 m Ali site ($32.306°$ north, $80.046°$ east) in late October 2017. The experimental scenes are shown in Figures 1 and 2.

The specifications of the AMIRM are given in Table 1; all optical elements except double sealing windows of the equipment were cooled to $-40°$C.

Fig. 1 The experimental scene at the Ali site.
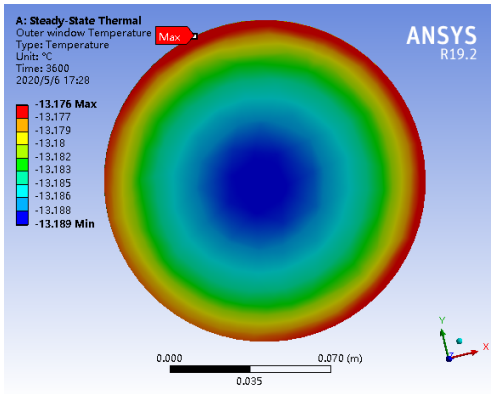

Fig. 2 The experimental scene at the Daocheng site.

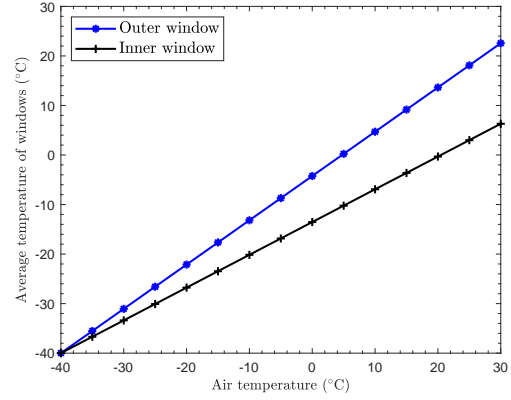

Fig. 3 Nephogram of outer window temperature.

Fig. 4 Window temperature with air-temperature.

Table 1 The Specifications of AMIRM

Equipment	Parameter	Value
Optical system	Aperture (cm)	7.5
	Focal length (cm)	15
	Operating temperature (°C)	-40 ± 0.02
	Filter spectral response (μm)	$4.605 \sim 4.755$
HgCdTe detector	Operating temperature (°C)	-196.15
	Spectral response (μm)	$3.7 \sim 4.8$
	Pixel pitch (μm)	30
	Format (pixel)	320×256

Our filter lies within the spectral range of the $\mathrm{M}'(4.57\,\mu\mathrm{m} \sim 4.79\,\mu\mathrm{m})$ filter at Mauna Kea Observatories (MKO, Leggett et al. 2003). Hereafter, M' means the spectral response between $4.605\,\mu\mathrm{m}$ and $4.755\,\mu\mathrm{m}$.

3.1 Multivariate Calibration of the AMIRM

The sealing windows of the AMIRM are close to the air and far from the cooler which is at $-40°\mathrm{C}$, so the temperature of the windows is significantly affected by air-temperature. Figure 3 shows that the simulating temperatures of the outer window are affected by the air-temperature of $-10°\mathrm{C}$.

Figure 4 illustrates that the simulating average temperatures of the windows vary with air temperature and are far higher than $-40°\mathrm{C}$ under the usual air-temperature conditions. Hence, calibration is necessary to eliminate the fluctuating thermal radiation of the windows. In the M'-band, the multivariate equation (Zhao 2017) obtained by calibrating in a temperature environmental chamber is shown in Equation (15):

$$I_{\mathrm{adu}} = 4.875 \times 10^5 \cdot t \cdot L_{\mathrm{sky}}^{M'} + 8.489 \times 10^3 \cdot t \cdot L_{\mathrm{amb}}^{M'}$$
$$+ 2.549 \cdot t + 707,$$

(15)

where I_{adu} is the reading (the unit is in ADU) of the AMIRM, t is exposure time, $L_{\mathrm{sky}}^{M'}$ is radiance of sky, $L_{\mathrm{amb}}^{M'}$ is black-body radiance at the air-temperature. The rms error of Equation (15) is 4.25 ADU.
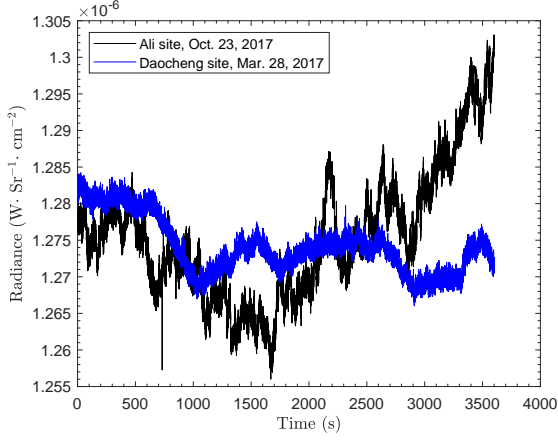
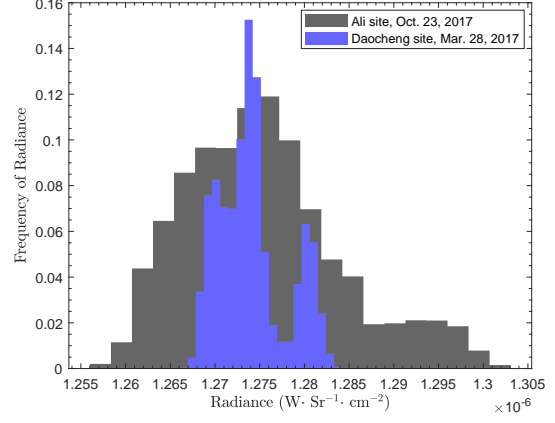**Fig. 5** Time sequence of sky brightness at two sites.
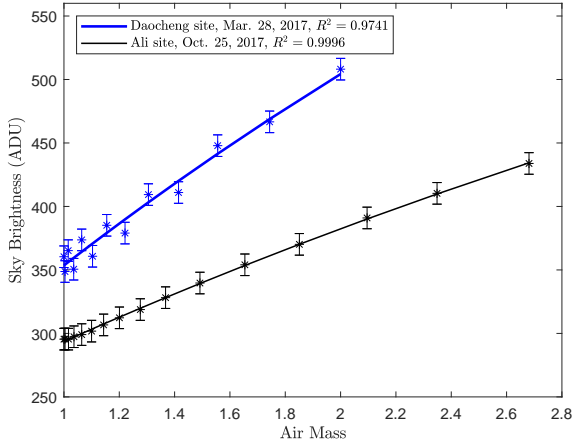

Fig. 6 Histogram of sky brightness at two sites.
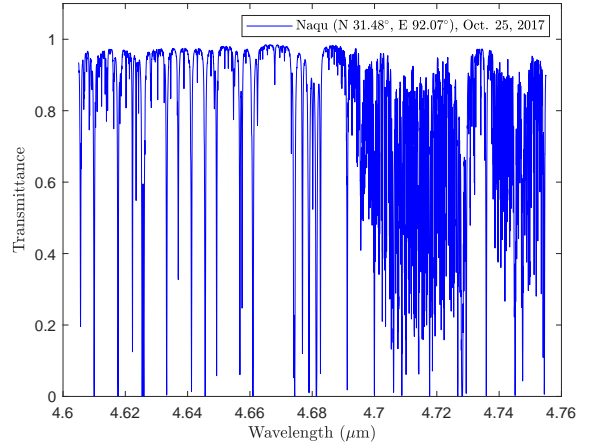

Fig. 7 Fitting sky brightness at different air mass.

Fig. 8 Transmittance calculated by LBLRTM.
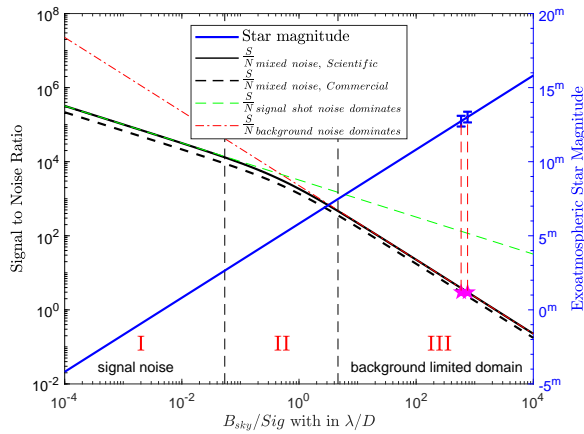

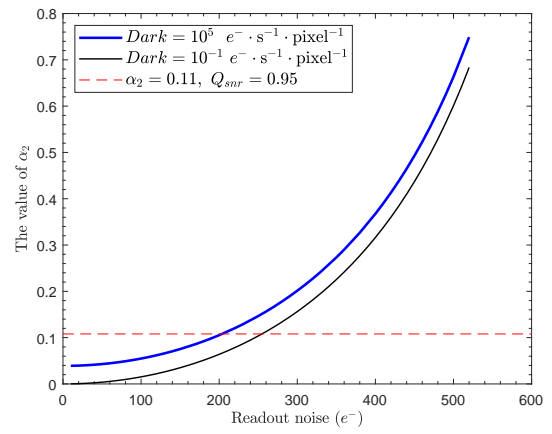**Fig. 9** S/N and magnitudes of 10 m telescopes at Ali.

Fig. 10 The effects of detector noise at Ali.

3.2 The Measured Sky Brightness at the Ali and Daocheng Sites

In Figure 5 we illustrate a one-hour sequence of the M'-band at the darkest sky brightness of the zenith which had

been measured from 21:35 (6:00) to 22:35 (7:00) Beijing time at Ali (Daocheng). The low frequency fluctuations of sky brightness are the sky noise usually subtracted
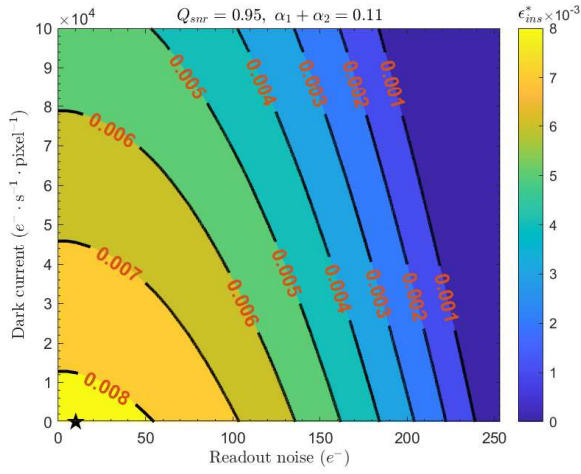
Fig. 11 The distribution of noise between a detector and instruments at Ali.
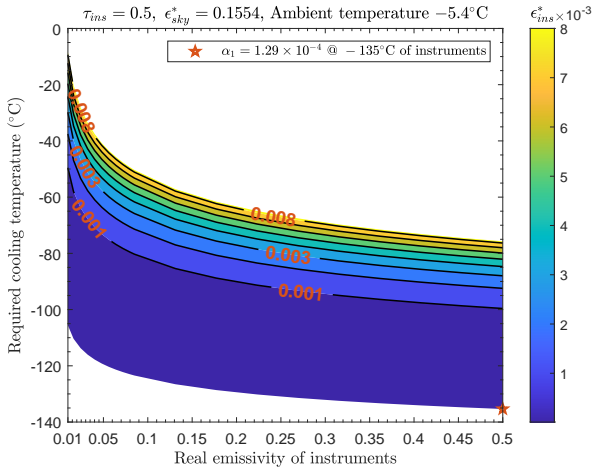

Fig. 12 The thermal-control of instruments at Ali.

by a chopping technique in the infrared astronomical observations.

The histogram for the above time sequence is shown in Figure 6, and the mean, standard deviation, minimum, and maximum are shown in Table 2. The M′-band sky brightness at Mauna Kea is also listed as a reference in Table 2, which is calculated by us based on the simulated data of spectral (between 4.605 μm and 4.755 μm) emission of the sky on Gemini Observatory's website[1](Lord 1992).

The spectral flux of the M′-band zero magnitude is 2.2×10^{-15} W · cm^{-2} · μm^{-1} (Léna et al. 2012). Thus, the magnitude per square arc-second of the mean sky brightness in Table 2 is 2.867 mag · arcsec^{-2} at Ali, 2.868 mag · arcsec^{-2} at Daocheng, and 2.064 mag · arcsec^{-2} at Mauna Kea.

Table 2 Statistics of the One-hour Sequence of M′-band Sky Brightness

Site	Value ($\times 10^{-6}$ W · Sr^{-1} · cm^{-2})			
	Maximum	Minimum	Mean	Standard deviation
Ali	1.303	1.256	1.275	0.009
Daocheng	1.284	1.266	1.274	0.004
Mauna Kea*	–	–	2.670	–

*Calculated by using the data with a water vapor column of 1.0 mm and an air mass of 1.0.

Table 3 The M′-band Atmospheric Extinction

Site	Atmospheric extinction at unit air mass (mag · airmass^{-1})
Ali	0.20
Daocheng	0.25
Mauna Kea (Leggett et al. 2003)	0.23

3.3 The Measured Atmospheric Extinction at the Ali and Daocheng Sites

The apertures of equipment used to measure the thermal infrared atmospheric radiation are usually very small. Therefore, it is generally impossible to measure atmospheric extinction using infrared standard stars in astronomical site surveys. For this reason we present a convenient method for the thermal infrared-band to measure extinction based on the atmospheric radiation transfer equation, as shown in Equation (16) (Zhao et al. 2018; Wang et al. 2020):

$$I_{\text{sky}} = a \cdot (1 - e^{-\overline{O}_d \cdot AM}), \qquad (16)$$

where I_{sky} is ADU readings of M′-band sky calibrated by Equation (15), AM is air mass at any zenith angles, and $\overline{O}_d$ is the average optical depth in M′-band at the zenith.

Figure 7 shows that the measured sky brightness at different air masses is fit by Equation (16), and the $\overline{O}_d$ obtained by fitting is 0.18 at Ali, and 0.23 at Daocheng. From $e^{-\overline{O}_d \cdot AM}$, the transmittance at the zenith is 0.84 at Ali and 0.80 at Daocheng. As a reference, by using LBLRTM (Line-By-Line Radiative Transfer Model), we calculate the spectral transmittance at the zenith with radiosondes data of Naqu[2], and the transmittance results are shown in Figure 8. By integrating the spectral transmittance in M′-band, the mean transmittance is 0.82 at Naqu.

The atmospheric extinction can be calculated by

$$\Delta m_{\text{ext}} = m_{\text{atm}} - m_{\text{exoatm}}$$
$$= -2.5\log_{10}(e^{-\overline{O}_d \cdot AM}) \approx 1.086 \times \overline{O}_d \cdot AM, \qquad (17)$$

Table 4 Input Parameters for Calculating M′-band S/N and Magnitudes

Type of parameter	Parameter name	Value	
Observational parameters	Total exposure time (s)	1	
	Elementary exposure time (s)	$1.6 \times 10^{-5} \sim 2.6 \times 10^{-1}$ @ 70% well fill	
Equipment specifications	Telescope+Relay optics transmittance	Photometry: 0.5	
	Quantum efficiency of detector	0.85	
	Full-well capacity of detector (e^-)	$\sim 10^6$	
	Dark electrons ($e^- \cdot s^{-1} \cdot pixel^{-1}$)	10^{-1} @ $-243°$C	10^5 @ $-143°$C
	RMS readout noise (e^-)	10	500

Table 5 Limiting Magnitudes of 10 m Telescopes without Instrumental Emission

Site	Scientific detector			Commercial detector			$m_{3\sigma}^{\mathrm{BLCAS}}$
	α_2	Q_{snr}	$m_{3\sigma}$	α_2	Q_{snr}	$m_{3\sigma}$	
Ali	1.5026×10^{-4}	0.9999	13.0122^{m}	0.6633	0.7755	12.7361^{m}	13.0123^{m}
Daocheng	1.5026×10^{-4}	0.9999	12.9596^{m}	0.6634	0.7755	12.6835^{m}	12.9597^{m}
Mauna Kea	1.5018×10^{-4}	0.9999	12.5716^{m}	0.6305	0.7832	12.3063^{m}	12.5716^{m}

where m_{atm} is the magnitude through the atmosphere, and m_{exoatm} is the magnitude beyond the atmosphere. Atmospheric extinctions at a unit air mass calculated by Equation (17) are given in Table 3.

The results of atmospheric extinction at Ali and Daocheng are slightly different from MKO because the wave-band of our filter is narrower than MKO's.

4 THE SENSITIVITY RESULTS AND DISCUSSION

In this section we first test the sensitivity model by calculating the M′-band limiting magnitudes of 10 m telescopes at the above three sites and then discuss the problem of detector selection and instrumental thermal-control. The involved input parameters are listed in Table 4, and two infrared detectors with different levels are chosen for comparison. $Dark = 0.1\ e^- \cdot s^{-1} \cdot pixel^{-1}$ and $Ron = 10\ e^-$ are parameters of the scientific detector used on Keck II (McLean 2003). $Dark = 10^5\ e^- \cdot s^{-1} \cdot pixel^{-1}$ and $Ron = 500\ e^-$ represent the noise level of commercial infrared detectors[3] (Rubaldo et al. 2016). The required site parameters are from Tables 2 and 3.

4.1 M′-band Limiting Magnitudes of 10 m Telescopes

Under the circumstances that an infrared telescope is used at its diffraction limit, we have that $\Omega_{\mathrm{star}} = \pi(1.22\lambda/D)^2$. According to Equation (4), the electrons per second at a unit pixel from the sky background at Ali, Daocheng, and Mauna Kea are about 2.567×10^6, 2.565×10^6, and 5.376×10^6 respectively. If an airy disk is resolved at the Nyquist frequency, $n_{\mathrm{pixel}} \approx 4$ and $\alpha_2 = 4 \times (Dark \cdot t + Ron^2)/(\tau_{\mathrm{ins}}\eta L_{\mathrm{sky}}\pi^2(0.61\lambda)t\frac{\lambda}{hc})$. The limiting magnitude at $S/N = 3$ is denoted by $m_{3\sigma}$. Under the condition that the instrumental emission is ignored ($\alpha_1 = 0$), we

---

[3] *https://www.lynred.com/products*

calculate the $m_{3\sigma}$ by Equations (2) and (9), which is shown in Table 5. The curves that relate S/N and magnitudes at Ali are shown in Figure 9, where the two five-pointed stars mean $S/N = 3$.

In Table 5, $m_{3\sigma}^{\mathrm{BLCAS}}$ is 3σ magnitude limited by the atmosphere. The scientific detector has little impact on the limiting magnitude, which is less than 0.0001^{m} at all three sites. The commercial detector has a significant impact on the limiting magnitude, which is about 0.3^{m}.

As discussed in Section 2.2, for $Q_{\mathrm{snr}} \geq 0.95$, the calculated 3σ magnitudes are greater than 12.956^{m}, 12.904^{m}, and 12.516^{m} at Ali, Daocheng, and Mauna Kea respectively, which decrease at most by 0.056^{m} relative to $m_{3\sigma}^{\mathrm{BLCAS}}$. Obviously, the Q_{snr} can clearly reflect whether the sky background limited sensitivity is approached. Hence, based on the requirements of observations, we can easily select appropriate detectors using Q_{snr}. Figure 10 shows the α_2 varying with different detector noise and the curve of $\alpha_2 = 0.11$ determined by $Q_{\mathrm{snr}} = 0.95$.

From Figure 10 we should select the detector such that the readout noise is less than $250\ e^-$ for $Dark = 10^{-1}\ e^- \cdot s^{-1} \cdot pixel^{-1}$, and $200\ e^-$ for $Dark = 10^5\ e^- \cdot s^{-1} \cdot pixel^{-1}$. The dark current just provides a small contribution to α_2 because it is far less than the sky background electrons (about $2.6 \times 10^6\ e^- \cdot s^{-1} \cdot pixel^{-1}$) in M′-band for the above two detectors. The dark current significantly decreases with decreasing the temperature of detectors. Therefore, for deep cryogenic detectors, we should pay special attention to readout noise.

4.2 The Discussion on Noise Distribution and Instrumental Thermal-Control

For thermal infrared observations, in addition to detector noise, we should also strictly control instrumental thermal emission, which is determined by the real emissivity

Table 6 The Required Cooling Temperature of Instruments for $Q_{\mathrm{snr}} = 0.95$

Site	The cooling temperature (°C)		
	$\epsilon_{\mathrm{ins}} = 0.01$	$\epsilon_{\mathrm{ins}} = 0.25$	$\epsilon_{\mathrm{ins}} = 0.5$
Ali @ −5.4°C	−29.47	−79.03	−87.18
Daocheng @ −10°C	−29.50	−79.05	−87.19

and temperature of the instruments. By using the above analysis, we can select a deep cryogenic detector such that the dark current can be ignored and the readout noise is $200\ e^-$. According to the measured sky brightness in Table 2 and Equation (6), the effective emissivity of sky is 0.1554 of −5.4°C at Ali, and 0.1898 of −10°C at Daocheng. In order to meet $Q_{\mathrm{snr}} \geq 0.95$, based on Equation (7) and the readout noise of $200\ e^-$, the effective emissivity of instruments should be less than 0.003 at Ali, and less than 0.004 at Daocheng. Obviously, if the real emissivity is equal to the effective emissivity, it is not necessary to refrigerate the instruments. For three instruments with given real emissivity, the required cooling temperatures are also calculated by Equation (6), which are shown in Table 6.

In Table 6, all elements have the same cooling temperatures for ease of calculation. However, the open-air elements of a telescope are hard to cool down to the same temperature as the relay optics. Therefore, the relay instrument should be cooled down to a lower temperature than in Table 6, and the real emissivity of the telescope should be kept as low as possible.

By taking the case of Ali site we calculate more possible combinations of detector noise and instrument noise, which are shown in Figure 11. The required cooling temperatures of instruments that vary with the instrumental real emissivity are calculated by Equation (6), which are shown in Figure 12.

The black five-pointed star in Figure 11 presents the noise of the scientific detector on Keck II. The red-brown five-pointed star in Figure 12 demonstrates that the instrumental thermal noise can be ignored for the instruments cooled down to −135°C. From the above two figures, when the thermal emission of instruments is strictly controlled, we are allowed to choose a less-than-ideal detector whose maximum readout noise is about $250\ e^-$. In other words an excellent thermal-control design of instruments makes it easier to select a required detector.

5 CONCLUSIONS

In this paper we constructed a sensitivity model used for the guidance of large telescope site surveys, detector selection, and instrumental thermal-control. The model was tested with the measured M'-band sky brightness and

atmospheric extinction in western China, and then the sensitivities limited by the atmosphere for 10 m telescopes were estimated. According to a given requirement of observational sensitivity, we discussed the principles of noise distribution and the problem on instrumental thermal-control. The better a site is, the more one needs to choose an excellent detector and strictly control instrumental thermal emission. When the instrument noise can be ignored, readout noise should still be less than $250\ e^-$. For Ali or Daocheng, if we choose a detector such that the readout noise is $200\ e^-$ and the dark current can be ignored, in order to fulfill $Q_{\mathrm{snr}} \geq 0.95$, the instruments whose real emissivity is 0.5 should be cooled to below −87.2°C.

If the statistical results of long-term data on sky brightness and atmospheric extinction are obtained, the model may be used to evaluate more objectively the sensitivity of large telescopes in a given infrared-band at any site and to guide the detector selection and the instrumental thermal-control effectively.

References

Ashley, M. C. B., Burton, M. G., Storey, J. W. V., et al. 1996, PASP, 108, 721

Cui, X., Zhu, Y., Liang, M., et al. 2018, in SPIE Conference Series, 10700, Ground-based and Airborne Telescopes VII, eds. H. K. Marshall, & J. Spyromilio, 107001P

Deng, Y., Liu, Z., Qu, Z., Liu, Y., & Ji, H. 2016, in Astronomical Society of the Pacific Conference Series, 504, Coimbra Solar Physics Meeting: Ground-based Solar Observations in the Space Instrumentation Era, eds. I. Dorotovic, C. E. Fischer, & M. Temmer, 293

Dong, S.-c., Wang, J., Tang, Q.-j., et al. 2018, Review of Scientific Instruments, 89, 023107

Feng, L., Hao, J.-X., Cao, Z.-H., et al. 2020, RAA (Research in Astronomy and Astrophysics), 20, 080

Leggett, S. K., Hawarden, T. G., Currie, M. J., et al. 2003, MNRAS, 345, 144

Léna, P., Rouan, D., Lebrun, F., Mignard, F., & Pelat, D. 2012, Observational Astrophysics (Springer Berlin Heidelberg)

Liu, Z., Deng, Y., Jin, Z., & Ji, H. 2012, in SPIE Conference Series, 8444, Ground-based and Airborne Telescopes IV, eds. L. M. Stepp, R. Gilmozzi, & H. J. Hall, 844405

Liu, Y., Li, X., Zhang, X., et al. 2018, in SPIE Conference Series, 10704, Observatory Operations: Strategies, Processes and Systems VII, 1070422

Lord, S. D. 1992, NASA Technical Memorandum, 103957

McLean, I. S. 2003, in SPIE Conference Series, 4834, Discoveries and Research Prospects from 6- to 10-Meter-Class Telescopes II, ed. P. Guhathakurta, 111

Phillips, A., Burton, M. G., Ashley, M. C. B., et al. 1999, ApJ, 527, 1009

Qian, X., Yao, Y., Wang, H., et al. 2015, in Journal of Physics Conference Series, 595, Journal of Physics Conference Series, 012028

Rubaldo, L., Brunner, A., Guinedor, P., et al. 2016, in SPIE Conference Series, 9755, Quantum Sensing and Nano Electronics and Photonics XIII, ed. M. Razeghi, 97551X

Smith, C. H., & Harper, D. A. 1998, PASP, 110, 747

Song, T.-F., Liu, Y., Wang, J.-X., et al. 2020a, RAA (Research in Astronomy and Astrophysics), 20, 085

Song, T. F., Cai, Z. C., Liu, Y., et al. 2020b, MNRAS, 499, 1909

Tang, Q.-J., Wang, J., Dong, S.-C., et al. 2018, Journal of Astronomical Telescopes, Instruments, and Systems, 4, 046002

Wang, F.-X., Xu, F.-Y., Guo, J., et al. 2020, RAA (Research in Astronomy and Astrophysics), 20, 134

Wang, H., Yao, Y., & Liu, L. 2013, Acta Optica Sinica, 33, 0301006

Wang, J., Zhang, Y. H., Tang, Q. J.,et al. 2018, in Ground-based and Airborne Telescopes VII

Westphal, J. A. 1974, Infrared Sky Noise Survey (NASA Technical Reports, NGR-05-002-185)

Wu, N., Liu, Y., & Zhao, H. M. 2016, Acta Astronomica Sinica, 57, 729

Yao, Y. 2005, Journal of Korean Astronomical Society, 38, 113

Zhao, Z.-J. 2017, Research on Background Radiation Characteristics of Ground-based Infrared Solar Observation, PhD Thesis, University of Chinese Academy of Sciences

Zhao, Z.-J., Xu, F.-Y., Wei, C.-Q., & Yang, K. 2018, Infrared Technology, 40, 718